Applied Thermal Engineering 143 (2018) 350–357

Contents lists available at ScienceDirect

Applied Thermal Engineering

journal homepage: www.elsevier.com/locate/apthermeng

Enhanced thermal performance of micro heat pipes through optimization of wettability gradient

Manjinder Singh[a], Naresh Varma Datla[a], Sasidhar Kondaraju[b], Supreet Singh Bahga[a,*]

[a] Department of Mechanical Engineering, Indian Institute of Technology Delhi, Hauz Khas, New Delhi 110016, India
[b] School of Mechanical Sciences, Indian Institute of Technology Bhubaneswar, Bhubaneswar, Odisha 751019, India

HIGHLIGHTS

- Optimization of wettability gradient for best thermal performance of a heat pipe.
- Optimization leads to 90% increase in the heat transfer rate of micro heat pipe.
- Optimal wettability gradient is independent of the fluid charge.
- Explanation of the underlying physical mechanism.

ARTICLE INFO

Keywords:
Micro heat pipe
Mixed wettability
Optimization
Surface treatment
Heat transfer enhancement

ABSTRACT

The use of wettability gradients has emerged as a promising method of enhancing the heat transfer capacity of micro heat pipes (MHPs). In this approach, a wettability gradient is created on the inner surface of an MHP such that the contact angle increases from the evaporator to the condenser section. Previous studies have shown up to 30% enhancement of thermal performance of MHPs by considering step-wise and linearly varying wettability gradient. However, previously chosen wettability gradient did not give the best possible performance as these wettability gradients were chosen arbitrarily. In this work, we perform a formal mathematical optimization of wettability gradient to show over 90% enhancement in the heat transfer capacity of the MHP under the constraints of maximum and minimum value of the contact angle. The MHP with optimal wettability gradient has uniformly high wetting evaporator and uniformly low wetting condenser. The primary gradient in wettability lies in the adiabatic section. We also show that the optimal wettability gradient is almost independent of the fluid charge. Lastly, we explain the physical mechanism underlying the enhanced thermal performance of the MHP with optimal wettability gradient.

1. Introduction

Micro heat pipes (MHP) are heat transfer devices that can passively remove heat of the order $10\,\mathrm{W m^{-2}}$ [1,2]. MHPs offer a promising thermal management solution for future microelectronic devices with high integration density [3–5]. A typical MHP, shown in Fig. 1, consists of an evacuated tube with sharp corners and is filled with a certain amount of working fluid. The working fluid resides in the corners in liquid state, whereas the vapor occupies the inner core region. An MHP is designed to have three sections namely evaporator, adiabatic and condenser sections. Heat added to the evaporator section vaporizes the liquid present in the corners, while the vapor condenses in the cooler condenser section. As a result, vapor pressure increases in the evaporator and decreases in the condenser. This gradient in vapor pressure drives the flow of vapor from the evaporator to the condenser via the adiabatic section. Evaporation in the evaporator and condensation in the condenser causes the liquid to recede in the corners of the evaporator and accumulate in the condenser section, as illustrated in Fig. 1(b) and (d), respectively. Receding of the liquid-vapor interface in the evaporator leads to a decrease in the radius of curvature of liquid-vapor interface. In contrast, the advancing liquid-vapor meniscus in the condenser section causes the radius of curvature of the interface to increase. This difference of meniscus curvature results in an axial pressure gradient within the liquid, resulting in the liquid flow from the condenser towards the evaporator.

With ever increasing thermal management requirements of microelectronic devices, various efforts have been made to improve the performance of MHPs [6–11]. The thermal performance of an MHP

* Corresponding author.
E-mail address: bahga@mech.iitd.ac.in (S.S. Bahga).

https://doi.org/10.1016/j.applthermaleng.2018.07.093
Received 2 April 2018; Received in revised form 17 July 2018; Accepted 17 July 2018
Available online 21 July 2018
1359-4311/

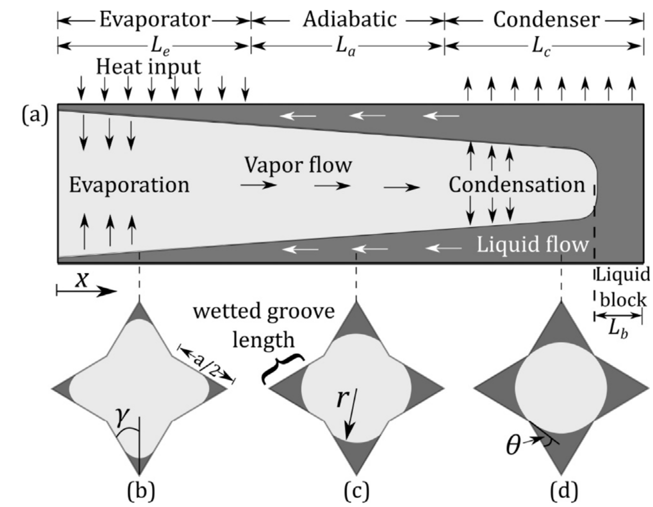

Fig. 1. Schematic illustrating operation of an MHP with trapezoidal cross-section. (a) Heat input to the evaporator section causes the liquid in the corners of evaporator section to evaporate. The increased vapor pressure in the evaporator section drives the vapor to the condenser via the adiabatic section. The vapor condenses to liquid in the condenser section and rejects the latent heat. The increased amount of liquid in the condenser section (d) leads to larger radius of curvature of liquid meniscus compared with that in the evaporator (b) and the adiabatic sections (c). Consequently, an axial gradient in capillary pressure develops which drives the liquid back to the evaporator, thereby completing the working cycle of MHP.

depends on various factors such as its geometry and the working fluid. Therefore, various studies have been conducted on optimization of geometry and working fluid to enhance the heat transfer capacity of MHPs. For example, Do et al. [12] optimized the width to height ratio of rectangular grooves of an MHP to obtain 20% enhancement in the heat transport capacity over a previous experimental study by Hopkins et al. [13]. An optimal geometry exists due to the competing effects of increased capillarity and higher hydraulic resistance upon narrowing the groove. The optimal choice of working fluid has been discussed in detail by Reay and Kew [14]. According to Reay and Kew, the working fluid should be chosen so as to maximize the Merit number (defined as $\sigma\rho_l h_{fg}/\mu_l$) where σ, ρ_l, h_{fg} and μ_l respectively denote surface tension, density, latent heat of vaporization and viscosity of the working liquid. As the thermophysical properties (σ, ρ_l, h_{fg} and μ_l) of a liquid depend on the temperature, the Merit number also depends on the temperature. Based on the largest Merit number criterion, water is preferred choice for the temperature range of 50–80 °C and ammonia is a better choice for the temperature range of 30–50 °C.

Apart from choosing the optimal groove geometry and the working fluid, the heat transfer capacity of an MHP can also be enhanced by changing the wettability of the inner surface of MHP. Recently Hu et al. [15] and Singh et al. [16] have shown that, the heat transfer capacity of MHP can be enhanced by creating an axial wettability gradient in the MHP with more wetting evaporator and less wetting condenser. Hu et al. [15] experimentally demonstrated that, compared to the grooved heat pipe with uniformly high wettability (contact angle, $\theta = 20°$), decreasing the wettability of the inner surface of the heat pipe from evaporator to condenser (from $\theta = 20°$ to $\theta = 85°$) enhances heat transfer capacity by 40%. Singh et al. [16] presented first ever mathematical model for MHP with wettability gradient and used it to explain the physical mechanism of heat transfer enhancement. In their theoretical analysis, Singh et al. considered five different wettability schemes; MHP with uniformly high wettability ($\theta = 10°$), MHP with uniformly low wettability ($\theta = 50°$), MHP with linear wettability gradient (10°–50°), and MHPs with step change in wettability (10°–10°–50°) and (10°–50°–50°) from evaporator to adiabatic to condenser section. Based on the theoretical model they predicted that among the chosen wettability schemes, the MHP with linearly increasing contact angle from evaporator to condenser has the highest heat transfer capacity. In particular, Singh et al. showed that linear variation of wettability from the evaporator to the condenser section (10°–50°) leads to 30% increase in the heat transfer capacity compared to the MHP with uniformly high wetting surface ($\theta = 10°$). Following these studies, Cheng et al. [17] carried out a detailed experimental and theoretical investigation into the effect of wettability gradient on the thermal performance of a grooved heat pipe. In their study Cheng et al. analysed grooved heat pipes with uniformly high wettability (contact angle, $\theta = 20°$), heat pipe with step change in wettability gradient (20°–45°–85°) and heat pipe with high wetting evaporator ($\theta = 20°$), low wetting condenser ($\theta = 85°$) and having a continuous axial variation of contact angle in the adiabatic section (20°–85°). Cheng et al. reported that among the various heat pipes considered, the heat pipe with a uniformly high wetting evaporator, uniformly low wetting condenser and having a continuous axial variation of contact angle in the adiabatic section has the least thermal resistance. These studies demonstrate that tuning the wettability of the inner surface of MHP is an additional way for improving the thermal performance of MHP, over and above the choice of proper geometry and working fluid.

Wettability gradients can be generated in MHPs made from a wide range of materials including silicon, copper, metals and ceramics. Huang et al. [18] developed an alkali assisted surface oxidation process for copper that was subsequently used by Hu et al. [15] for the enhanced thermal performance of a miniature heat pipe. In this method, the copper substrate is immersed in an aqueous solution of $(NH_4)_2S_2O_8$ and NaOH and drawn out at a specific rate. Because the contact angle decreases with the immersion time, by correctly choosing the withdrawing rate desired wettability gradients can be generated. To generate wettability gradients on silicon, silanization [19] and contact printing of octadecyltrichlorosilane on oxidised silicon wafers [20] can be used. The silanization process involves diffusion of volatile dodecyltrichlorosilane on a silicon wafer which forms a self-assembled mono-layer (SAM) of variable concentration. In the contact printing method, the wettability gradient is generated by varying the contact time between the substrate surface and elastomeric stamp inked with octadecyltrichlorosilane. For generating wettability on ceramics, the dip coating process [21] can be used. The dip coating process is very easy to scale up and can also be used on metallic surfaces. In this process, the wettability gradient is obtained by first immersing the substrate into a precursor solution (alkoxide in alcohol solvent) followed by withdrawal at a constant rate. The solvent (alcohol) evaporates leaving behind a thin layer of alkoxide of variable thickness. Given the recent experimental evidence of enhanced thermal performance of MHPs with wettability gradients [15,17] along with availability of various surface treatment methods, MHPs with gradient wettability is a promising technology for micro electronics cooling. However, unlike those for geometry and working fluid, no formal optimization study has been performed till now on selecting the best wettability gradient for obtaining the highest heat transfer capacity of an MHP.

In this paper, we present mathematical optimization of wettability gradient to maximize the heat transfer capacity of an MHP under the constraints of maximum and minimum wettability allowable by the surface treatment methods. We consider two cases for optimization in which: (i) the mass of the working fluid is fixed, that is, mass is a constraint and (ii) the mass of the working fluid is a design variable. Based on our optimization analysis, we obtain the axial wettability gradient at which the MHP has the highest thermal performance. We also compare the heat transfer capacity of MHP with optimal wettability gradient with that of MHPs with wettability gradient that have been studied previously, such as linear wettability gradient (10°–55°) and uniform wettability (10°). Our calculations show that the optimization of wettability gradient, under the constraints of same maximum and minimum contact angles, leads to more than 90% increase in the heat transfer capacity compared to the MHP with uniform high wettability ($\theta = 10°$) and more than 20% compared to the MHP with linear wettability gradient (10°–55°). We also provide the physical reasoning of why the optimal wettability gradient leads to highest heat transfer capacity of the MHP.

2. Mathematical modelling

The maximum heat transfer capacity of any heat pipe is governed by various physical limits, such as the sonic, viscous, entrainment, and capillary limits. The maximum heat transport rate corresponding to sonic (Q_s), viscous (Q_{vis}) and entrainment (Q_e) limits have been provided by Reay and Kew [14] and are respectively given by

$$Q_s = A_v \rho_v h_{fg} (\gamma_v R_v T_v)^{1/2} / (2(\gamma_v + 1))^{1/2}, \tag{1a}$$

$$Q_{vis} = r_v^2 h_{fg} \rho_v p_v A_v / 16 \mu_v L_E, \text{ and} \tag{1b}$$

$$Q_e = A_v h_{fg} \sigma \rho_v^{1/2} / (2d)^{1/2}. \tag{1c}$$

Here A, L and $d = (4A)/(\text{perimeter})$, respectively denote the fluid flow area, length and the vapor phase hydraulic diameter of the MHP. The subscripts v and E respectively represent the vapor phase and the effective length ($L_E = L_a + (L_e + L_c)/2$) of the MHP, where L_e, L_a and L_c denote the lengths of the evaporator, adiabatic and condenser sections. In the present study, we are only concerned with the capillary limit, as MHPs are usually limited by the capillary limit [22]. Capillary limit corresponds to the operating condition at which the axial gradient in pressure is no longer sufficient to overcome the hydraulic loss in the MHP corners. A comparison of various limits (see Fig. 6) posed on the maximum heat transfer capacity, presented later in Section 3.5, shows that even in MHP with wettability gradient the heat transport capacity is limited by the capillary limit. Therefore, throughout we will discuss the model for only capillary limit.

The mathematical model to analyse the steady-state characteristics, in the capillary limit, of a regular-polygonal shaped MHP with N corners and treated for an axial wettability gradient has been discussed in detail in our previous work, Singh et al. [16]. Here, we briefly outline the important governing equations and the solution strategy for calculating the maximum heat transfer capacity of the MHP in the capillary limit. We assume the MHP to be isothermal as the change in the operating temperature T across the length of MHP is typically less than 1 K. We consider contact angle variation along the axis of the MHP that varies from 10° in the evaporator to 55° in the condenser. The wettability of surface with contact angles from 10° to 55° does not have a significant effect on the condensation and evaporation processes [23,24]. Therefore, we neglect the effect of wettability of the inner surface of MHP on evaporation and condensation processes. We also make an assumption that the contact angle made by the working liquid with the surface is equal to the local static contact angle. That is, we neglect the contact angle hysteresis. This assumption is reasonable as contact angle hysteresis is usually an order of magnitude small compared with the static contact angles [19,20,25–28]. For the same reason, the assumption of zero contact angle hysteresis has been used in the majority of studies on modelling of MHPs [22,29–31]. Following Singh et al. [16], the rate of heat transfer $Q(x)$ along the axial direction as a function of distance x from the beginning of evaporator is given by

$$Q(x) = \begin{cases} \frac{x}{L_e} Q_{in}, & 0 \leqslant x \leqslant L_e \\ Q_{in}, & L_e \leqslant x \leqslant L_e + L_a \\ Q_{in}\left(1 + \frac{L_e + L_a - x}{L_{eff,c}}\right), & L_e + L_a \leqslant x \leqslant L_e + L_a + L_{eff,c}, \end{cases} \tag{2}$$

where subscripts e, a, and c denote evaporator, adiabatic and condenser sections, respectively. In Eq. (2), Q_{in} denotes the total heat input and $L_{eff,c}$ denotes the effective length of the condenser section. The effective length of the condenser section $L_{eff,c}$ accounts for the formation of liquid block due to overcharging of the MHP, as shown in Fig. 1. The effective length of the condenser section is defined as

$$L_{eff,c} = L_c - L_b, \tag{3}$$

where L_b is the length of the liquid block, as illustrated in Fig. 1(a). Under steady state conditions, the mass flow rate of liquid $\dot{m}_l$ and vapor $\dot{m}_v$ are given by the energy balance,

$$\dot{m}_l = -\dot{m}_v = \frac{Q(x)}{h_{fg}}. \tag{4}$$

The liquid flow inside the MHP is characterised by low Reynolds number, ($Re \ll 1$) wherein inertial effects are negligible and viscous effects dominate. Also, the long and slender geometry of the MHP ensures that the liquid flow can be assumed to be quasi-one-dimensional. Therefore, the liquid pressure gradient causing the flow of liquid from the condenser to the evaporator is given by the lubrication approximation of Navier–Stokes equations as [29]

$$\frac{\mathrm{d}p_l}{\mathrm{d}x} = \frac{2\mu_l fRe \dot{m}_l}{\rho_l A_l N D^2}. \tag{5}$$

Here fRe is the Poiseuille number defined as the product of friction factor f and Reynolds number Re at a given cross-section. The Poiseuille number fRe depends on the local contact angle. Therefore, to obtain the value of fRe along the axial length of MHP, we use a correlation derived from the numerical results of Ayyaswami et al. [32]. In Eq. (5), A_l is the local liquid cross-sectional area and D is the hydraulic diameter of the liquid cross-section. A_l and D depend on the radius of curvature of the liquid-vapor interface as

$$A_l = Nr^2\left[\cot(\gamma + \theta) - \left(\frac{\pi}{2} - (\gamma + \theta)\right) + \frac{\cot(\gamma + \theta)\cos(\gamma + \theta)\sin(\theta)}{\sin(\gamma)}\right], \tag{6}$$

$$D = \frac{A_l}{2r\cos(\gamma + \theta)}, \tag{7}$$

where θ is the local contact angle and γ is the half angle of the triangular groove as depicted in Fig. 1. For detailed derivations of Eqs. (6) and (7), the readers are referred to Singh et al. [16]. Eqs. (6) and (7) show that the liquid flow area and the hydraulic diameter at an axial location depend on the local wettability of the inner surface of MHP. For a given radius of curvature of the liquid-vapor interface, the liquid flow area is smaller for a low wettability surface (large θ) compared with high wettability surface (small θ). Therefore, by tuning the local wettability of the surface along the axis of MHP, the liquid flow area can be altered which in turn affects the hydraulic resistance and the liquid distribution in the MHP.

Unlike for the liquid flow, inertial effects cannot be neglected for the vapor flow as the Reynolds number for vapor flow is not small ($Re > 1$). To account for the inertial effects, we use the relation for vapor pressure drop provided by Faghri et al. [33]

$$\frac{\mathrm{d}p_v}{\mathrm{d}x} = \begin{cases} 2\left(-8|Re_e| - \frac{16}{3}Re_e^2\right)\left(\frac{\mu_v^2}{\rho_v R^4}\right)x, & 0 \leqslant x \leqslant L_e \\ \left(\frac{-8\mu_v \bar{u}_{v,a}}{R^2}\right), & L_e \leqslant x \leqslant L_e + L_a \\ 2\left(-8|Re_c| - \frac{16}{3}Re_c^2\right)\left(\frac{\mu_v^2}{\rho_v R^4}\right)x + \left(\frac{16}{3}|Re_c| - 8\right)\left(\frac{\mu_v \bar{u}_{v,a}}{R^2}\right), \\ \quad L_e + L_a \leqslant x \leqslant L_e + L_a + L_{eff,c}, \end{cases} \tag{8}$$

where R denotes half of the local hydraulic diameter of the vapor region. In this equation, Re_c and Re_e are dimensionless numbers that respectively denote radial Reynolds number in the condenser and evaporator section, and $\bar{u}_{v,a}$ is the mean velocity of vapor flow in the adiabatic section, defined as

$$Re_e = \frac{\dot{m}_{v,a}}{2\pi L_e \mu_v}, \quad Re_c = \frac{\dot{m}_{v,a}}{2\pi L_c \mu_v}, \quad \bar{u}_{v,a} = \frac{\dot{m}_{v,a}}{\rho_v \pi R^2}. \tag{9}$$

The above expression for vapor pressure drop has been used in several studies on MHP, including studies by Kim et al. [29] and Singh et al. [16].

The liquid in an MHP flows due to the pressure gradient generated by the variation in radius of curvature of the liquid-vapor interface from the condenser to the evaporator section. The pressure in the liquid phase is related to the radius of curvature of the liquid-vapor meniscus by the Young–Laplace equation

$$p_v - p_l = \frac{\sigma}{r}. \tag{10}$$

In this equation, we have neglected the axial radius of curvature as it is significantly large as compared with the lateral radius of curvature r. The capillary limit of MHP occurs when the mass flow rate of liquid from the condenser to the evaporator due to the liquid pressure gradient is less than the rate of evaporation of the liquid in the evaporator. At this stage, the beginning of the evaporator dries out and the radius of curvature of liquid-vapor interface at the evaporator inlet approaches zero. The heat input at dry out is the maximum heat transfer capacity of the MHP in the capillary limit. Therefore, to calculate the maximum heat transfer capacity of MHP we need to find the liquid pressure gradient. Eqs. (5)–(7) show that the liquid pressure gradient depends on the radius of curvature r and the local contact angle θ. The contact angle is a predefined parameter and therefore the calculation of liquid pressure gradient requires the radius of curvature r of the liquid-vapor interface along the length of MHP. To this end, we differentiate Eq. (10) with respect to x to obtain the differential equation for r,

$$\frac{dr(x)}{dx} = \frac{r(x)^2}{\sigma}\left(\frac{dp_l}{dx} - \frac{dp_v}{dx}\right). \tag{11}$$

The liquid and vapor pressure gradients are related to the corresponding mass flow rates by Eqs. (5) and (8) which in turn are related to the heat input $Q(x)$ from Eq. (4). Therefore, knowing the heat input Q_{in}, Eq. (11) can be integrated to obtain the axial variation of radius of curvature.

2.1. Numerical method

Eq. (11) is a non-linear equation and it does not permit an analytical solution. Therefore, for a known value of heat input, we solve Eq. (11) numerically. We discretize the domain equally into n grid points and integrate Eq. (11) using fourth order Runge–Kutta scheme. For solving Eq. (11), we require one boundary condition in the form of radius of curvature at the beginning of the evaporator section. In the capillary limit, the radius of curvature at the beginning of the evaporator is zero corresponding to dryout. However, this boundary condition leads to a singularity while solving Eq. (11). Therefore, we choose a vanishingly small value $r(0) = r_{min}$ such that the maximum heat transport capacity corresponding to the capillary limit is not affected. For our calculations, a value of $r_{min} = 0.02 \times r_{max}$ suffices. Here, r_{max} denotes the radius of curvature of the interface when the liquid completely wets the groove and is given by

$$r_{max} = \frac{a}{2}\frac{\sin(\gamma)}{\cos(\gamma + \theta)}. \tag{12}$$

We note that the value of r_{max} used to calculate the r_{min} is computed corresponding to wettability of the surface at the condenser end ($\theta = 55°$). In practice, we use the following approach to obtain the heat transport capacity of the MHP in the capillary limit for a given wettability gradient and fluid charge m_o. For a given value of Q_{in}, Eqs. (5), (8) and (11) are solved using the boundary condition $r(0) = r_{min}$. From the resulting variation of radius of curvature, mass of the fluid is calculated using

$$m = \int_0^L \rho_l A_l dx + \int_0^L \rho_v (A - A_l) dx. \tag{13}$$

By performing these calculations at different values of Q_{in} we obtain the heat transfer capacity in the capillary limit for corresponding mass of working fluid m_o, that is $Q_{in} = Q_{in}(\theta_1, \theta_2, ..., \theta_n, m_o)$. For all our calculations, we put an additional constraint that the radius of curvature at any axial location is less than r_{max}, ($r \leqslant r_{max}(\theta)$). If the radius of curvature at all points beyond a certain location exceeds r_{max}, the MHP is assumed to be completely filled with liquid beyond that location. We note that for an MHP working below the capillary limit and charged with mass less than its ideal mass, the radius of curvature at evaporator beginning is chosen iteratively such that the calculated mass of working fluid, given by Eq. (13), is equal to the actual fluid mass of MHP m_o. For an MHP charged with ideal mass of working fluid, the liquid block just begins to form at the condenser end, that is, $r(L) = r_{max}(\theta(L))$ at condenser end is r_{max}.

2.2. Optimization

In this paper, we present an optimization of the wettability gradient $\theta = \theta(x)$ to obtain the highest heat transfer capacity of the MHP with wettability gradient in the capillary limit. We perform the optimization for two cases in which the mass of the working fluid: (i) is fixed and hence a constraint and (ii) is a design variable. The contact angle $\theta = \theta(x)$ is allowed to vary between $\theta_{min} = 10°$ and $\theta_{max} = 55°$. Practically, θ_{min} and θ_{max} are dictated by the surface treatment method. Here we have choosen $\theta_{min} = 10°$ and $\theta_{max} = 55°$ to compare our results with the results of previous work on MHP with wettability gradient by Singh et al. [16]. As the axial length of the heat pipe is discretized into n grid points, contact angle at each grid point, $(\theta_1, \theta_2, ..., \theta_n)$, act as a variable. The optimization problem is defined as obtaining that value of contact angle θ_i at every grid point that maximizes the heat transfer capacity of the MHP in the capillary limit. When the fluid charge is fixed at m_o, the optimization problem is formulated as

$$\text{Case 1:} \quad \max_{\{\theta_i\}_{i=1}^{n}} Q_{in} = Q_{in}(\theta_1, \theta_2, ..., \theta_n), \tag{14}$$

The contact angle at n discrete points $\{\theta_i\}_{i=1}^{n}$ are subject to

$$\theta_{min} \leqslant \theta_n \leqslant \theta_{max} \text{ and,} \quad m = m_o \tag{15}$$

where $Q_{in}(\theta)$ is the maximum possible heat input such that the radius of curvature $r(x)$ for all locations is $r(x) \leqslant r_{max}(\theta(x))$ for a given wettability gradient. The constraint on the mass of working fluid for the case wherein MHP is charged with a fixed mass of working fluid is already incorporated into the numerical method, as discussed in Section 2.1. In case of MHP charged with ideal mass of the working fluid that is when fluid charge m is a design variable, the optimization problem is formulated as

$$\text{Case 2:} \quad \max_{\{\theta_i\}_{i=1}^{n}, m} Q_{in} = Q_{in}(\theta_1, \theta_2, ..., \theta_n, m), \tag{16}$$

The contact angle at n discrete points $\{\theta_i\}_{i=1}^{n}$ are subject to

$$\theta_{min} \leqslant \theta_n \leqslant \theta_{max}, \tag{17}$$

The heat transport capacity depends implicitly on the design variables which complicates the calculation of derivatives for optimization. Therefore, we use a derivative free approach based on the interior point algorithm [34] to optimize the wettability gradient. The algorithm starts from an initial feasible point. At each iteration, the interior point algorithm solves the Karush–Kuhn–Tucker (KKT) equations [35] through a linear approximation. The KKT equations are the necessary conditions analogous to the first derivative test which states that gradient of a function is zero at a minimum and maximum.

We used the "fmincon" function in MATLAB for performing optimization using the interior point method. During optimization, choosing θ at all n grid points as design variables is computationally expensive. Therefore, we choose contact angle θ at lesser number of equally spaced grid points j (<n) along the axis of the MHP. The contact

Table 1
Geometrical parameters of the MHP used in the current work.

Parameter	Value
Evaporator section length, L_e	13 mm
Adiabatic section length, L_a	31 mm
Condenser section length, L_c	13 mm
Groove side length, $a/2$	0.33 mm
Half angle, γ	30°
Number of grooves, N	4

angles θ at the remaining grid points are obtained by fitting the data at j grid points using shape preserving cubic hermite polynomial. This curve fitting approach eliminates unwanted overshoots and undershoots during interpolation.

3. Results and discussion

To demonstrate the effect of optimal wettability gradient on the performance of MHP, we performed optimization of wettability gradient for a trapezoidal MHP filled with water as the working fluid. For all our calculations, we used thermo-physical properties of water taken from NIST chemistry web-book [36]. The geometric parameters of the trapezoidal MHP are given in Table 1. This MHP design, shown in Fig. 1, is same as that used by Wu and Peterson [37] in their experimental work. To find the maximum heat transfer capacity of the MHP for a given wettability gradient, the length of MHP is discretized into $n = 570$ grid points. However, as described in Section 2.2, we use contact angles at $j = 20$ equally spaced grid points as the design variables for optimization. The contact angles at remaining grid points were obtained through interpolation. Our numerical experiments show that increasing the number of design variables beyond $j = 20$ does not lead to an appreciable change in the results of optimization.

3.1. Optimal wettability gradient for fixed mass of working fluid

We first present the results of optimization when the fluid charge is fixed at 3.2 mg of water. This particular value was chosen to compare our results with the experiments of Wu and Peterson [37], who used an MHP with the same geometry, working fluid and the mass of working fluid. The experimental study of Wu and Peterson provides data of maximum heat transfer for varying operating temperatures, with which we have validated our model. Before we discuss our numerical results, we provide an overview of the experimental methodology of Wu and Peterson. In their experimental study, Wu and Peterson [37] used two copper trapezoidal MHPs with uniform wettability. The geometrical dimensions of the MHP are given in Table 1. One MHP was charged with 3.2 mg of distilled water whereas the other MHP was left uncharged. The solid-liquid combination of copper-water had a contact angle of 55°. The uncharged heat pipe was used to evaluate the heat conducted through the walls to determine the improvement in heat transfer capacity of the MHP when charged with fluid. The onset and termination of dryout at a given operating were identified as that values of heat input at which conductance of the MHP changed most rapidly with respect to temperature. The rate of heat transfer corresponding to the onset and termination of dryout at a given temperature is respectively shown using solid and hollow circles in Fig. 2.

The optimal wettability gradient under the constraint that the maximum and minimum contact angles are 55° and 10° is shown in Fig. 2(a). We performed the optimization at the operating temperature of 333 K for the gradient shown in Fig. 2(a). Performing optimization at different operating temperatures shows that the optimal wettability gradient does not change appreciably with the operating temperature. The axial variation of wettability obtained after the optimization shows that the MHP with optimal thermal performance has uniformly high wetting surface up to a length of 25 mm from the evaporator inlet. The length of MHP up to 25 mm covers the evaporator section and a part of the adiabatic section. Beyond the distance of 25 mm from the evaporator beginning and up to the end of the adiabatic section (44 mm) the wettability of the MHP varies almost linearly from $\theta = 10°$ to $\theta = 50°$. In the condenser section, the wettability of the inner surface effectively is uniformly low wetting ($\theta = 55°$). Fig. 2(b) shows the maximum heat transfer rate of MHPs with optimal wettability gradient, linear wettability gradient of Singh et al. [16], uniformly high wettability (10°) and uniformly low wettability (55°) at varying operating temperatures. In Fig. 2, we also compare the model predictions with the experimental data of Wu and Peterson [37]. For $\theta = 55°$, the predictions of our model compare well with experimental data of Wu and Peterson which serve as a validation of the model. Our calculations show that, compared with an MHP having uniformly high wettability ($\theta = 10°$), treating the MHP for optimal wettability gradient leads to more than 65% increase in the maximum heat transfer capacity at operating temperature of $T = 333$ K. Moreover, the heat transport capacity of the MHP with optimal wettability gradient is 15% higher than that with a linear wettability gradient proposed by Singh et al. [16]. Note that, here we have followed the approach of Kim et al. [29], and Hung and Seng [30] and assumed uniform heat flux in the evaporator and condenser sections. In practice, as shown by Hung and Tio [31], axial variations in interfacial resistance may lead to corresponding variations in heat flux in the evaporator and condenser sections. However, our calculations show that making the assumption of uniform heat flux in evaporator and condenser sections yields less than 10% difference compared with the alternate approach of modelling phase-change interfacial resistances to obtain the heat flux [31].

3.2. Physical mechanism

To elucidate the physical mechanism underlying the enhancement in the thermal performance through optimization of wettability gradient, in Fig. 3(a)–(c) we respectively compare the axial variation of r, A_l and p_l for MHPs with uniformly high wettability ($\theta = 10°$) and optimal wettability gradient. We performed these calculations for Q_{in}= 0.6 W, a fluid charge of 3.2 mg and at an operating temperature of 333 K. The heat input Q_{in}= 0.6 W corresponds to the maximum heat transfer capacity Q_{max} of MHP with uniformly high wettability. As shown in Fig. 3(a), under steady-state operating conditions the radius of curvature of the liquid-vapor interface increases monotonically from the evaporator to the condenser section for the MHP with uniform $\theta = 10°$. This corresponds to the recession of liquid in the evaporator and accumulation of the liquid in the condenser leading to a monotonic increase in the liquid flow area from the evaporator to the condenser section, as shown in Fig. 3(b). Consequently, for the MHP with uniform $\theta = 10°$, the liquid flow area in the evaporator section is smaller than that in the condenser and adiabatic sections. Because of the lower liquid flow area in the evaporator section majority of the hydraulic loss in the MHP occurs in the evaporator section, as shown in Fig. 3(c). A favorable wettability gradient reduces the hydraulic loss by redistributing the working fluid from the condenser to the evaporator section. This is because, for an MHP with a high wetting evaporator and a low wetting condenser section, the working liquid is preferentially located in the evaporator section. Therefore, a wettability gradient that ensures maximum redistribution of liquid from the condenser to the evaporator section will result in reduced hydraulic loss and enhanced heat transport capacity.

Similar to the MHP with uniform $\theta = 10°$, the radius of curvature for MHP with optimal wettability gradient increases monotonically along the axial direction (Fig. 3(a)). This is required to ensure that liquid flows back to the evaporator. However, the corresponding variation of liquid flow area in Fig. 3(b) shows that the liquid flow area does not increase monotonically as in the case of MHP with uniform wettability. Instead, for the MHP with optimal wettability gradient, the liquid flow area decreases near the condenser section leading to a redistribution of liquid to the evaporator section. This can be explained using Eq. (6),

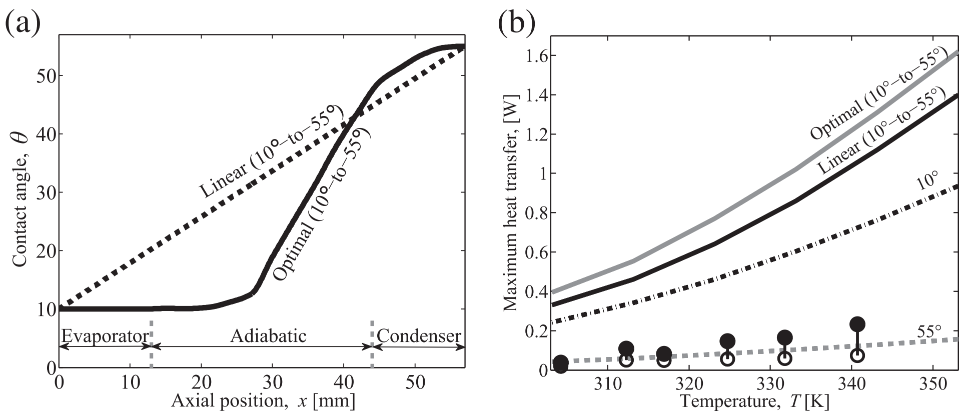

Fig. 2. Optimal wettability gradient and its effect on the maximum heat transfer capacity of MHP. (a) The optimal wettability gradient in comparison to the linear wettability gradient at operating temperature of 333 K. (b) The maximum heat transfer capacity of the MHPs with optimal wettability gradient, linear wettability gradient (10° to 55°), uniformly high wettability (10°) and uniformly low wettability (55°) at various operating temperatures. Experimental data of the Wu and Peterson [37]: (○) on-set of dryout; (●) termination of dryout. The calculations are performed for MHP filled with 3.2 mg of water as working fluid.

which shows that the liquid flow area depends on the radius of curvature and the local contact angle. The liquid flow area increases with the radius of curvature whereas the effect of an increase in the contact angle is to reduce the liquid flow area. For the surface with uniform wettability, the liquid flow area varies only with the radius of curvature. As a result, the monotonic increase in the radius of curvature in MHP with uniform wettability is accompanied by a monotonic increase in the liquid flow area along the MHP axis. However, the magnitude of the liquid flow area along the axis of MHP with optimal wettability gradient is determined by the competing effects of increasing radius of curvature of liquid-vapor interface and decreasing contact angle.

Fig. 3(a) and (b) show that for the optimal wettability gradient despite an increase in the radius of curvature along the axis of MHP, the liquid flow area does not increase monotonically. Instead, the liquid in the condenser is redistributed to the evaporator from the condenser. Therefore, for the same heat input, the radius of curvature and the liquid flow area in the evaporator is higher and correspondingly the drop is lower (Fig. 3(c)) for MHP with optimal wettability gradient than that for MHP with uniform wettability. The larger radius of curvature at the evaporator inlet suggests that the MHP with optimal wettability gradient is less prone to dry out, as higher heat input can be provided before the working fluid present in evaporator dries out. In conclusion,

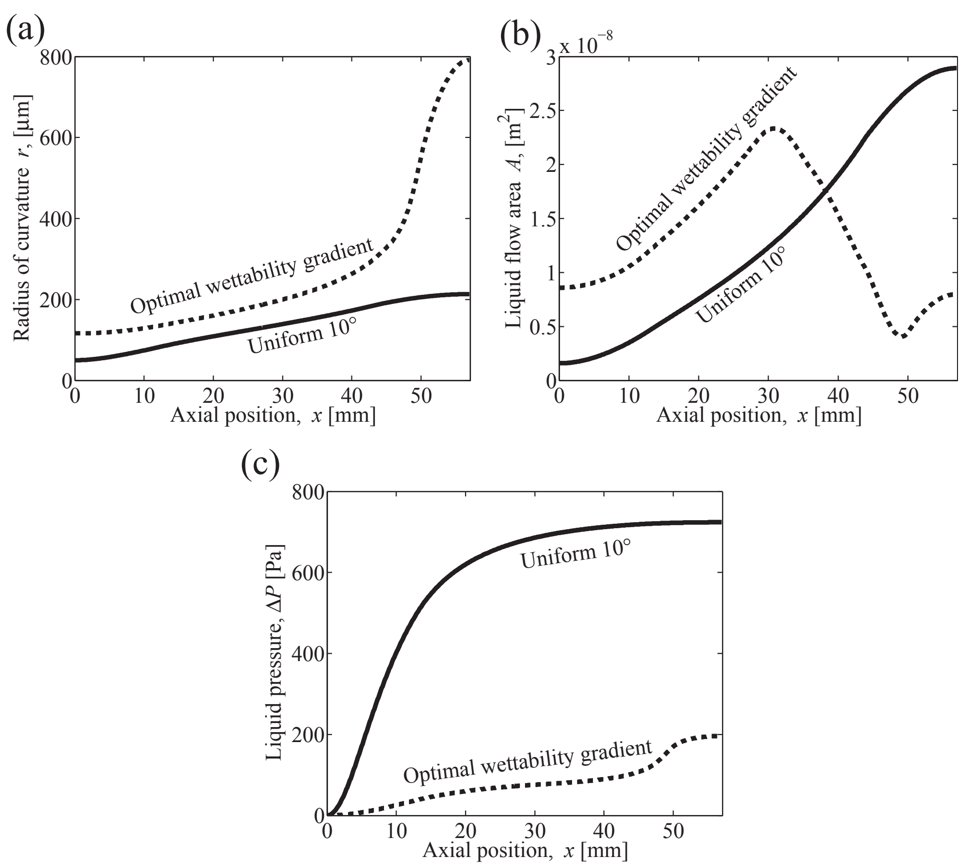

Fig. 3. Effect of surface wettability on the variation of radius of curvature, pressure and liquid flow area along the length of MHP. Axial variation of (a) the radius of curvature of the liquid-vapor meniscus, (b) the liquid flow area and (c) liquid pressure for MHP with uniformly high wettability (θ = 10°) and MHP with optimal wettability gradient. Compared with MHP having uniformly high wettability θ = 10°, the radius of curvature at the evaporator inlet (x = 0) is higher for MHP with optimal wettability gradient, suggesting that it is less prone to dry-out. The liquid flow area increases monotonically in case of MHP with a uniform wettability. However, for the MHP with optimal wettability gradient, the liquid flow area decreases in the condenser section resulting in redistribution of the liquid from the condenser to the evaporator. These calculations are based on 0.6 W of heat input and 3.2 mg of water as the working fluid.

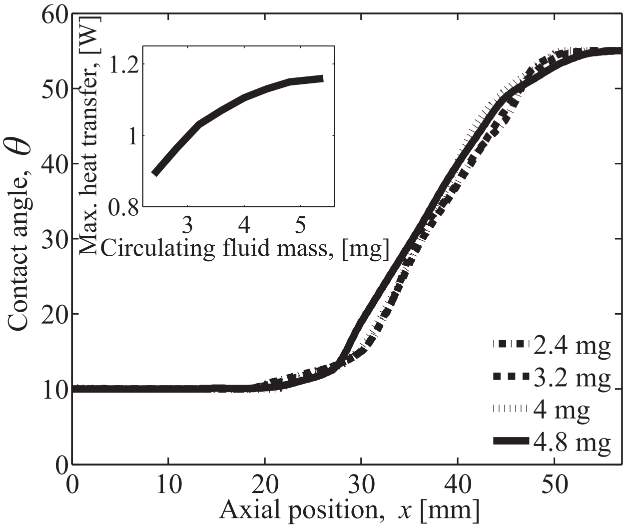

Fig. 4. Effect of working fluid mass on the optimal wettability gradient and corresponding maximum heat transfer capacity of the MHP. These calculation were performed at operating temperature of 333 K. The optimization results show that the optimal wettability gradient does not vary appreciably with the fluid charge.

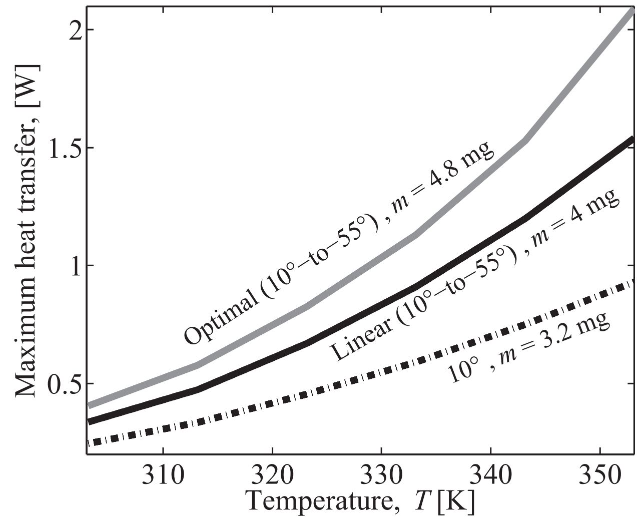

Fig. 5. Effect of different surface wettability on the maximum heat transfer capacity of the MHP at various operating temperatures in case of MHP charged with an ideal mass of working fluid. The ideal mass of working fluid for an MHP changes with wettability of its inner sarface. The optimal wettability gradient yields higher heat transport capacity than other wettability schemes.

the optimal wettability gradient ensures maximum redistribution of the liquid to the evaporator section thereby delaying the dryout.

3.3. Effect of mass of the working fluid on optimal wettability gradient

Next, we analyze whether the optimal wettability gradient is specific to the mass of working fluid. In Fig. 4, we present the effect of mass of working fluid on the optimal wettability gradient at a fixed operating temperature of 333 K. The inset in Fig. 4 shows the corresponding heat transfer capacity of the MHP in the capillary limit. The results show that the optimal wettability gradient does not change appreciably with the mass of the working fluid. This is expected because the best thermal performance of an MHP with a fixed mass is obtained corresponding to an optimal wettability gradient that ensures maximum redistribution of the liquid mass from the condenser to the evaporator section. In other words, it is the relative redistribution of mass from the condenser to the evaporator and not the absolute mass of the fluid that governs the optimal wettability gradient. Further, Fig. 4 shows that the heat transfer capacity in the capillary limit increases with the increase in the mass of working fluid. At lower fluid mass ($m = 2.4$ mg) the heat transfer capacity in the capillary limit of the MHP increases appreciably with an increase in the mass of working fluid. However, at higher fluid charge that is as the fluid mass approaches ideal fluid mass ($m = 4.8$ mg) improvement in the maximum heat transfer capacity reduces. This leveling off of the maximum rate of heat transfer can be attributed to the development of maximum capillary pressure across the MHP. This is because, with the increase in fluid charge the difference in the radius of curvature across the MHP approaches its maximum value. Further addition of liquid mass to the MHP, beyond the ideal fluid charge, leads to the formation of the liquid block which does not enhance the thermal performance of MHP.

3.4. MHP performance at ideal fluid charge and optimal wettability gradient

Till now we have presented the results of optimization while keeping the mass of working fluid fixed. However, the best thermal performance of an MHP is obtained when the MHP is charged with an ideal mass of the working fluid. Therefore, we now present optimization results for the case when the mass of working fluid is a design variable in addition to the wettability gradient. We perform the optimization at the operating temperature of 333 K. Fig. 5 shows the maximum heat transfer capacity of MHPs with optimal wettability gradient, linear wettability gradient and uniform high wettability each charged with the corresponding ideal mass of working fluid for the temperature range of 303–353 K. The values of ideal mass corresponding to these wettability schemes are also provided in Fig. 5. The optimal wettability gradient and the ideal mass does not vary appreciably over the temperature range shown in Fig. 5. Similar to the results discussed in Section 3.2, at all operating temperatures MHP with optimal wettability gradient and charged with the ideal mass of working fluid has the highest heat transfer capacity. Compared with the MHP with uniform high wettability and charged with its respective ideal mass (m= 3.2 mg), the MHP with optimal wettability gradient (m= 4.8 mg) has 90% higher heat transfer capacity at an operating temperature of 333 K. The enhancement in heat transfer capacity in case of MHP with optimal wettability gradient and charged with ideal mass is 20% more than the MHP charged with fixed mass 3.2 mg of working fluid. Moreover, compared with MHP having linear wettability gradient and charged with corresponding ideal mass (m = 4 mg), heat transfer capacity of the MHP with optimal wettability gradient is 20% higher.

3.5. Heat transfer limits of the MHP

As discussed in Section 2, the maximum heat transfer capacity of a heat pipe is governed by sonic, viscous, entrainment and capillary limits. There we emphasized that the thermal performance of an MHP with wettability gradient is limited by the capillary limit. Now, we show that maximum heat transfer capacity of the MHP obtained after optimization of wettability gradient does not exceed the heat transfer limitations posed by sonic, viscous, and entrainment limits and is indeed governed by the capillary limit. Fig. 6 shows the above mentioned four limits at various operating temperatures of the MHP. As shown in Fig. 6, the maximum heat transfer capacity of the MHP with optimized wettability gradient is still governed by the capillary limit and does not exceed the sonic, viscous and entrainment limits.

4. Conclusion

We have performed optimization of wettability gradient to enhance the maximum heat transfer capacity of an MHP with wettability

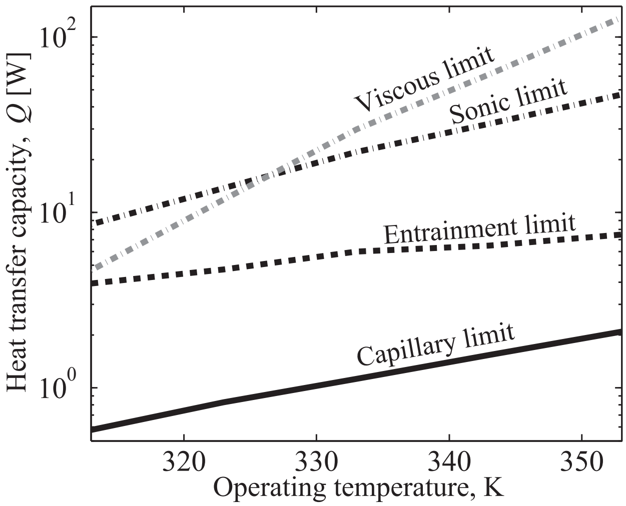

Fig. 6. Capillary, viscous, sonic and entrainment limits of the MHP with optimal wettability gradient and filled with water as working fluid at various operating temperatures. Clearly, the capillary limit governs the maximum heat transport capacity at all operating temperatures.

gradient, under the constraints that maximum contact angle $\theta_{max} = 55°$ (low wetting) and minimum contact angle $\theta_{min} = 10°$ (high wetting). We performed the calculations for MHPs filled with (i) a given mass of working fluid and (ii) an ideal mass of working fluid. The axial wettability gradient obtained after the optimization shows that MHP with the highest heat transfer capacity is the one in which the evaporator section is high wetting, the condenser section is low wetting and the adiabatic section have a continuous variation of contact angle from high wettability to low wettability. Our calculations show that compared with MHP having uniformly high wettability ($\theta = 10°$) and filled with a given mass of working fluid optimization of the wettability gradient leads to 65% enhancement in the heat transfer capacity of MHP. A similar comparison between MHP with uniformly high wettability and MHP with optimal wettability gradient each charged with the corresponding ideal mass of working fluid shows more than 90% increase in the maximum heat transfer capacity due to the optimization of wettability gradient. Our analysis shows that varying the mass of working fluid does not appreciably change the optimal wettability gradient.

We also explained the underlying physical mechanism that leads to the enhanced thermal performance of MHP with optimal wettability gradient. Making the evaporator high wetting and condenser low wetting disrupts the monotonic increase of liquid flow area from the evaporator to the condenser section and leads to a decrease in the liquid flow area in the condenser section. The decrease in the liquid flow area in condenser section results in redistribution of liquid from the condenser to evaporator section. Smaller variation in liquid flow area along the axis of MHP leads to lower hydraulic resistance and correspondingly higher heat transport capacity. In future, a complete optimization of an MHP can be done by simultaneously optimizing for geometry, working fluid and the wettability gradient.

Acknowledgments

S.K. thanks DST INSPIRE fellowship for providing necessary funds for carrying out this research.

Appendix A. Supplementary material

Supplementary data associated with this article can be found, in the online version, at https://doi.org/10.1016/j.applthermaleng.2018.07.093.

References

[1] T. Cotter, Principles and prospects of micro heat pipes, in: Proceedings of the Fifth Int. Heat Pipe Conference, Tsukuba, Japan, 1984, pp. 2051–2063.
[2] M. Mochizuki, T. Nguyen, K. Mashiko, Y. Saito, T. Nguyen, V. Wuttijumnong, A review of heat pipe application including new opportunities, Frontiers in Heat Pipes (FHP) 2 (2011).
[3] Y. Shabany, Heat Transfer: Thermal Management of Electronics, CRC Press, New York, 2009.
[4] J. Qu, H. Wu, P. Cheng, Q. Wang, Q. Sun, Recent advances in mems-based micro heat pipes, Int. J. Heat Mass Transfer 110 (2017) 294–313.
[5] S.-C. Wong, H.-S. Cheng, C.-W. Tu, Visualization experiments on the performance of mesh-wick heat pipes with differing wick wettability, Int. J. Heat Mass Transfer 114 (2017) 1045–1053.
[6] D. Reay, P. Kew, Heat Pipes, fifth ed., Butterworth-Heinemann, London, 2006.
[7] L. Bai, G. Lin, G. Peterson, Evaporative heat transfer analysis of a heat pipe with hybrid axial groove, J. Heat Transfer 135 (2013) 031503.
[8] Y.M. Hung, Q. Seng, Effects of geometric design on thermal performance of star-groove micro-heat pipes, Int. J. Heat Mass Transfer 54 (2011) 1198–1209.
[9] C. Zhang, Y. Chen, M. Shi, G. Peterson, Optimization of heat pipe with axial omega-shaped micro grooves based on a niched pareto genetic algorithm (npga), Appl. Therm. Eng. 29 (2009) 3340–3345.
[10] C. Ömür, A.B. Uygur, H.G. Işık, I. Horuz, Manufacturing phase embedded design optimization of extruded heat pipes for space applications, Appl. Therm. Eng. 126 (2017) 436–446.
[11] H. Tang, Y. Tang, W. Yuan, R. Peng, L. Lu, Z. Wan, Fabrication and capillary characterization of axially micro-grooved wicks for aluminium flat-plate heat pipes, Appl. Therm. Eng. 129 (2018) 907–915.
[12] K.H. Do, S.J. Kim, S.V. Garimella, A mathematical model for analyzing the thermal characteristics of a flat micro heat pipe with a grooved wick, Int. J. Heat Mass Transfer 51 (2008) 4637–4650.
[13] R. Hopkins, A. Faghri, D. Khrustalev, Flat miniature heat pipes with micro capillary grooves, J. Heat Transfer 121 (1999) 102–109.
[14] D. Reay, P. Kew, Heat Pipes, fifth ed., Butterworth-Heinemann, London, 2006.
[15] Y. Hu, J. Cheng, W. Zhang, R. Shirakashi, S. Wang, Thermal performance enhancement of grooved heat pipes with inner surface treatment, Int. J. Heat Mass Transfer 67 (2013) 416–419.
[16] M. Singh, S. Kondaraju, S.S. Bahga, Enhancement of thermal performance of micro heat pipes using wettability gradients, Int. J. Heat Mass Transfer 104 (2017) 400–408.
[17] J. Cheng, G. Wang, Y. Zhang, P. Pi, S. Xu, Enhancement of capillary and thermal performance of grooved copper heat pipe by gradient wettability surface, Int. J. Heat Mass Transfer 107 (2017) 586–591.
[18] Z. Huang, J. Zhang, J. Cheng, S. Xu, P. Pi, Z. Cai, X. Wen, Z. Yang, Preparation and characterization of gradient wettability surface depending on controlling $Cu(OH)_2$ nanoribbon arrays growth on copper substrate, Appl. Surface Sci. 259 (2012) 142–146.
[19] S. Daniel, M.K. Chaudhury, J.C. Chen, Fast drop movements resulting from the phase change on a gradient surface, Science 291 (2001) 633–636.
[20] S.H. Choi, B.Z. Newby, Micrometer-scaled gradient surfaces generated using contact printing of octadecyltrichlorosilane, Langmuir 19 (2003) 7427–7435.
[21] M. Faustini, D.R. Ceratti, B. Louis, M. Boudot, P.-A. Albouy, C. Boissiere, D. Grosso, Engineering functionality gradients by dip coating process in acceleration mode, ACS Appl. Mater. Interfaces 6 (2014) 17102–17110.
[22] B. Babin, G. Peterson, D. Wu, Steady state modeling and testing of a micro heat pipe, J. Heat Transfer 112 (1992) 595–601.
[23] X. Du, T. Zhao, Analysis of film condensation heat transfer inside a vertical micro tube with consideration of the meniscus draining effect, Int. J. Heat Mass Transfer 46 (2003) 4669–4679.
[24] M. Singh, S. Kondaraju, S.S. Bahga, Mathematical model for dropwise condensation on a surface with wettability gradient, J. Heat Transfer 140 (2018) 071502-071502-8.
[25] Y.-H. Lai, J.-T. Yang, D.-B. Shieh, A microchip fabricated with a vapor-diffusion self-assembled-monolayer method to transport droplets across superhydrophobic to hydrophilic surfaces, Lab on a Chip 10 (2010) 499–504.
[26] D. Hong, W.K. Cho, B. Kong, I.S. Choi, Water-collecting capability of radial-wettability gradient surfaces generated by controlled surface reactions, Langmuir 26 (2010) 15080–15083.
[27] J. Genzer, Surface-bound gradients for studies of soft materials behavior, Ann. Rev. Mater. Res. 42 (2012) 435–468.
[28] Y. Ito, M. Heydari, A. Hashimoto, T. Konno, A. Hirasawa, S. Hori, K. Kurita, A. Nakajima, The movement of a water droplet on a gradient surface prepared by photodegradation, Langmuir 23 (2007) 1845–1850.
[29] S. Kim, J. Seo, K. Do, Analytical and experimental investigation on the operational characteristics and the thermal optimization of a miniature heat pipe with a groovedwick structure, Int. J. Heat Mass Transfer 46 (2003) 2051–2063.
[30] Y. Hung, Q. Seng, Effects of geometric design on thermal performance of star-groove micro-heat pipes, Int. J. Heat Mass Transfer 54 (2011) 1198–1209.
[31] Y.M. Hung, K.-K. Tio, Thermal analysis of a water-filled micro heat pipe with phase-change interfacial resistance, J. Heat Transfer 134 (2012) 112901.
[32] P. Ayyaswami, I. Catton, D. Edwards, Capillary flow in triangular grooves, J. Appl. Mech. 41 (1974) 332–336.
[33] A. Faghri, Performance characteristics of a concentric annular heat pipe: Part II-vapor flow analysis, J. Heat Transfer 111 (4) (1989) 851–857.
[34] R.H. Byrd, M.E. Hribar, J. Nocedal, An interior point algorithm for large-scale nonlinear programming, SIAM J. Optim. 9 (1999) 877–900.
[35] J. Nocedal, S. Wright, Numerical Optimization, Springer-Verlag, New York, 1999.
[36] E. Lemmon, M. McLinden, D. Friend, Thermophysical properties of fluid systems, NIST chemistry webbook, NIST standard reference database 69, 2005.
[37] W. Wu, G. Peterson, Investigation of the transient characteristics of a micro heat pipe, J. Thermophys. 5 (2) (1991) 129–134.